Hybrid density functional theory study of vanadium monoxide

William C. Mackrodt,* Derek S. Middlemiss, and Thomas G. Owens
School of Chemistry, University of St. Andrews, St. Andrews, Fife KY16 9ST, Scotland, United Kingdom
(Received 2 August 2003; revised manuscript received 20 October 2003; published 24 March 2004)

First-principles calculations of nondefective VO in the $Fm\bar{3}m$ structure based on a range of single-particle Hamiltonians containing varying amounts of exact exchange indicate that the ground electronic state is that of a d^3 high spin, antiferromagnetic (AF), Mott-Hubbard insulator with an AF_1 spin alignment of the local cation moments. This description remains essentially unchanged down to 10% exact exchange, and only for the pure density functional theory (DFT) potential is the AF_1 phase found to be metallic. Strong spin-lattice interaction is predicted with differences in lattice constant of up to 1.6% between AF_1 and FM (ferromagnetic) order. The AF_1 lattice constant is predicted to be $\sim$4.37 Å, which is roughly 7% greater than the reported lattice constants for the defective material. The bulk modulus is comparable to those of CaO, MnO, and NiO. A mapping of total energies onto an Ising spin Hamiltonian containing both direct and superexchange interactions reveals the dominant magnetic interaction to be the direct coupling of antiferromagnetically aligned nearest-neighbor cation spins, which leads to the stability of the AF_1 phase. Direct coupling energies are found in the range -11.1 to -44.3 meV as the proportion of exact exchange is reduced, leading to an estimated critical disorder temperature in the range 300–450 K. However, the limitations of such mapping are exposed by a consideration of the relative stabilities of the AF_1 and AF_3 alignments. Orbital projected densities of states reveal filled to unfilled gaps which depend strongly on the proportion of exact exchange and for the B3LYP potential (20% exact exchange) are $\sim$2.5 eV for the spin-forbidden $xy(\uparrow)\rightarrow xy(\downarrow)$ excitation, $\sim$3.0 eV for $xy(\uparrow)\rightarrow z^2(\uparrow)$, and $\sim$3.5 eV for V$\rightarrow$O charge transfer. Variationally stable, highly local crystal-field excited states ranging in energy from $\sim$0.6 to $\sim$2.7 eV are predicted for exchange-correlation potentials down to 30% exact exchange and from comparisons with the corresponding band excitation estimates of $\sim$1 to $\sim$2 eV are obtained for the localization energy of Frenkel excitons. From a mapping of the excited crystal-field energies onto a Kanamori Hamiltonian, values are obtained for the lattice Racah B and C parameters and the d-orbital averaged exchange and crystal-field energies. A comparison of mapped and directly calculated energies of the two-electron excitation $(xz,yz)\rightarrow(z^2,x^2-y^2)$ confirms the validity of Kanamori mapping, notably in the limit of exact exchange.

DOI: 10.1103/PhysRevB.69.115119 PACS number(s): 71.20.−b, 71.27.+a, 71.35.−y, 75.25.+z

I. INTRODUCTION

Amongst the transition-metal oxides, those of the higher valence states of vanadium find diverse application as oxidation catalysts,[1] lithium insertion electrodes,[2] environmental sensors[3] and optical devices, and may even be formed into nanotubes.[4] Progress will inevitably be aided by an understanding of the electronic and magnetic structures of these systems, and while the complexity and subtlety of the fundamental properties of these systems continue to pose severe and particular difficulties for theory, a sound description of the structurally simpler lower oxide, vanadium monoxide, VO_x, will contribute usefully to an understanding of the full V-O phase diagram. To date, however, such a basic description has proved to be elusive, although the reasons for this are clear. Tight control of the stoichiometry, x, is difficult to achieve in addition to which VO_x is undoubtedly close to a Mott-Hubbard transition, while possessing a complex defect structure, over a wide composition range.

The structural and electrical characterization of VO_x has an interesting history. Early work suggested that at low temperature VO_x breaks down into a mixture of a body-centered tetragonal phase of composition V_3O and a V_3O_4 phase which is either body-centered cubic or body-centered tetragonal, with a c/a ratio close to unity.[5] Later work established that VO_x is structurally homogeneous in the $Fm\bar{3}m$ rocksalt lattice over a wide composition range, $0.8<x<1.3$.[6,7] X-ray crystallography of phases with differing compositions disclosed the presence of varying concentrations of vacancies on both cation and anion sublattices. Only for $x=1.0$ are the concentrations of both metal and oxygen vacancies equal, amounting to $\approx$15% of the available sites.[8] The lattice constant is found to increase across the homogeneity range, from $\approx$4.03 Å at $x=0.8$ to 4.13 Å at $x=1.3$ at room temperature, with values of 4.071 (Ref. 9) and 4.063 Å (Ref. 8) reported for the nominally stoichiometric phase, VO.

A metal to semiconducting phase transition has been reported at a critical temperature $T_0=125$ K (Refs. 10 and 11), although later authors[8,12] suggested that this transition in the earlier samples was due to the presence of V_2O_3. A study of the magnetic properties of the system found antiferromagnetic behavior for $x=1.25$ and 1.147 with critical temperatures of 7.0 and 4.6 K, respectively. Compositions with higher metal content display paramagnetic susceptibility, but no transitions associated with ordering of the atomic moments have been observed.[9,12]

In terms of electrical characterization, there is a large body of work which shows that VO_x displays metallic characteristics for $x<1$ and semiconductivity for $x>1$. Activation energies for electronic conduction have been obtained

which increase with x from 2×10^{-3} eV at $x=1.0$ to $\approx 50\times10^{-3}$ eV at $x=1.3$,[9,12–21] and variations in resistivity from 7×10^{-4} to 1 Ω cm in the range $-0.2<x<0.2$ at room temperature. Such behavior differs from that found in the structurally related compound TiO_x, which remains metallic throughout the stoichiometry range $0.75<x<1.3$, and undergoes a superconducting transition at low temperature. No superconductivity has been found in VO_x down to a temperature of 0.3 K. Measurements of the Seebeck coefficient α in VO_x show a change in sign at $x=1$, indicating conduction by holes for higher metal content and by electrons for higher oxygen content. The coexistence of charge carriers of opposite electrical polarity in VO_x has been confirmed by magnetoresistance studies.[21,22]

Historically, band theoretical methods of varying sophistication have been applied to the ideal $Fm\bar{3}m$ VO lattice. Early non-self-consistent calculations based on a linear combination of atomic orbitals (LCAO) tight-binding method, Slater's $\rho^{4/3}$ exchange potential,[23] and a series of *ad hoc* crystal potentials yielded a metallic ground state, with the Fermi energy lying in the V($3d$) band. A very broad d band of width ~ 7 eV was also predicted on the basis of the neutral atom potential.[24] These calculations were performed at the experimental lattice constant of the defective lattice, and made no allowance for spin polarization. Non-self-consistent augmented plane-wave (APW) calculations,[25] again at the defective lattice constant, with Slater exchange and *ad hoc* crystal potentials led to similar conclusions. A self-consistent APW study of the lighter transition-metal monoxides based on X_α exchange predicted VO to be a d-band metal, with a bandwidth of ~ 7.5 eV, at the observed lattice constant.[26] Self-consistent atomic sphere approximation calculations employing the local spin-exchange-correlation functional of von-Barth and Hedin[27] were conducted as a function of lattice constant,[28] and once again indicated a d-band metal with an approximate bandwidth of 8 eV. More recently, a first-principles spin-unrestricted Hartree-Fock (UHF) calculation based on localized atomic orbitals predicted VO to be a high spin antiferromagnetic Mott-Hubbard insulator, with an optimized lattice constant of 4.460 Å.[29]

Clearly there are fundamental differences between first-principles DFT and UHF calculations as to the nature of the ground state of the fully stoichiometric, nondefective $Fm\bar{3}m$ VO lattice, with, perhaps, even more profound differences for the technologically important higher oxides. This is an unsatisfactory situation in view of the success of both DFT and UHF methodologies in describing the ground states of a wide range of first-row transition-metal oxides. Here we report fresh studies of the ground state of VO, which we have extended to the $d\rightarrow d$ excited states, to shed light on some of these differences.

Initial insight into the ground state of fully stoichiometric, nondefective VO might be sought from a consideration of the d-band occupancies of the subgroup, CaO, VO, MnO, NiO, and ZnO, of the $Fm\bar{3}m$ oxides. Assuming comparable ionicities and crystal-field characteristics, the spin band occupancies can be written as

$$\mathrm{CaO}\ —,$$

$$\mathrm{VO}\ \ d^3_{t_{2g}}(\uparrow),$$

$$\mathrm{MnO}\ \ d^3_{t_{2g}}(\uparrow)d^2_{e_g}(\uparrow),$$

$$\mathrm{NiO}\ \ d^3_{t_{2g}}(\uparrow)d^3_{t_{2g}}(\downarrow)d^2_{e_g}(\uparrow),$$

$$\mathrm{ZnO}\ \ d^3_{t_{2g}}(\uparrow)d^3_{t_{2g}}(\downarrow)d^2_{e_g}(\uparrow)d^2_{e_g}(\downarrow).$$

Now CaO, MnO, NiO, and (presumably) ZnO with 0, 2, 3, and 4 completely filled spin bands, respectively, are all insulating, from which it might reasonably be concluded that VO with one completely filled spin band, $d^3_{t_{2g}}(\uparrow)$, would also be insulating. Furthermore, it might be anticipated that VO would display Mott-Hubbard (MH) characteristics within the Zaanen, Sawatzky, and Allen classification.[30] It is known, both from studies of the elemental transition metals and the oxides that the d band gradually falls in energy relative to the O($2p$) band and contracts spatially as it is filled, for the added electron cannot fully screen the increase in nuclear charge.[28] Therefore, charge-transfer behavior at the right of the transition series should give way to MH behavior at the left. Finally, it might also be expected that VO would exhibit antiferromagnetic spin alignment by comparison with the two magnetic members of the subgroup, MnO and NiO.

The failure of the local-density approximation (LDA) and to a limited extent the gradient corrected density functionals to correctly describe the insulating ground state of the majority of the late transition metal oxides is now widely acknowledged.[31–36] For example, the LDA predicts NiO to be a d-band metal, rather than the experimentally observed charge-transfer insulator. A small band gap is found in MnO only by virtue of the imposition of antiferromagnetic order, while it is known experimentally that the insulating state persists well above the Néel temperature. The introduction into the LDA of a potential, which depends on orbital occupation either through self-interaction correction[37,38] or from the imposition of an arbitrary U (LDA+U) (Refs. 39–41), seems to correct the grosser deficiencies of the purely local functionals, opening gaps at the Fermi level and increasing atomic moments. However, against these apparent limitations of DFT, at least within the local-density approximation, a relatively recent study of TiO_x has demonstrated the power and utility of this approach in describing the lattice structure of the nonstoichiometric phases of the $3d$ oxides.[42] It is apparent that, despite an inaccurate ground state, the LDA provides an acceptable account of the relative energetics of the structural phases.

Accordingly, to resolve some of these issues and to predict the magnetic characteristics of and elementary excitations in stoichiometric, nondefective VO prior to potential high-pressure studies, we have carried out a hybrid density-functional study of this system along the lines reported recently for MgO,[32] NiO,[32,43] and CoO.[32]

II. THEORETICAL METHODS

A. Hybrid DFT Hamiltonians

As discussed above, all previous DFT calculations for ideal VO have employed purely local functionals, in which the spurious self-interaction might be expected to cause unphysical effects. In contrast, in the UHF method, the Coulomb self-interaction is exactly canceled by self-exchange terms in the exchange series, so that the potential is truly dependent upon orbital occupancy. In an attempt to embody the advantages of both DFT and UHF methods in a unified single-particle approach, so-called hybrid methods have been developed, of which the B3LYP method is perhaps the most successful. This was originally developed to improve the theoretical thermochemistry of small molecules[44] and subsequently shown to yield molecular geometries[45] that are significant improvements over those obtained from currently available gradient corrected functionals. The difficulties involved in calculating the exact Fock exchange for periodic systems have now been overcome, and the B3LYP method has recently been applied to a number of solids, including the transition metal-oxides.[32,43,48]

The essence of the B3LYP method is that the exchange-correlation contribution to the Kohn-Sham Hamiltonian, f^{xc}_{B3LYP}, is given by

$$f^{xc}_{\mathrm{B3LYP}} = f^{x}_{B3} + 0.81 f^{c}_{\mathrm{LYP}} + 0.19 f^{c}_{\mathrm{VWN}},$$

where f^{c}_{LYP} and f^{c}_{VWN} are the correlation functionals of Lee, Yang, and Parr[46] and Vosko, Wilk, and Nusair,[47] respectively. The exchange functional f^{x}_{B3} is a weighted sum of exact UHF (f^{x}_{UHF}) and gradient-corrected local spin-density approximation (LSDA) ($f^{x}_{\mathrm{LSDA}} + 0.9\Delta f^{x}_{B88}$) (Ref. 44) contributions

$$f^{x}_{B3} = (1 - F_0)(f^{x}_{\mathrm{LSDA}} + 0.9\Delta f^{x}_{B88}) + F_0 f^{x}_{\mathrm{UHF}}$$

and F_0 an arbitrary weighting parameter. F_0 values of 1 and 0 correspond to exact exchange (UHF) and pure DFT descriptions, respectively, while a value of 0.2 corresponds exactly to Becke's original three-parameter exchange functional ($B3$).[44] It is this hybrid methodology that we have followed in the present study. Although the presence of only 20% of the exact exchange is not sufficient to cancel the Coulomb self-interaction, the method has been shown to yield values for the gaps between the filled O($2p$) and empty metal $3d$ states which are apparently in close agreement with experimental band gaps of varying provenance.[48] Optimized structural parameters are typically found to lie within a broad range of $\pm 2\%$ of the experimental values.

The approach we followed was to vary F_0 in the range $0 \leqslant F_0 \leqslant 1$, yielding a series of hybrid Hamiltonians, including the B3LYP ($F_0 = 0.2$). The specific values of F_0 used were 0.0, 0.1, 0.2, 0.4, 0.6, 0.8, and 1.0, thus allowing us to examine the effect of varying amounts of exact exchange on the electronic and magnetic properties of VO. In addition, and for comparison, UHF calculations without correlation were also carried out.

B. Ising spin Hamiltonian

To exploit further the calculations for the individual magnetic states, we have extracted direct, J_d, and superexchange, J_{se}, coupling constants by mapping the total energies of the FM, AF_1, and AF_2 alignments onto an Ising spin Hamiltonian of the form

$$\hat{H}_{\mathrm{Ising}} = \hat{H}^{0}_{\mathrm{Ising}} - \frac{J_d}{2}\sum_{ij}^{\mathrm{nn}} \sigma_i \sigma_j + \frac{J_{se}}{2}\sum_{ij}^{\mathrm{nnn}} \sigma_i \sigma_j ,$$

where the summations run over nearest neighbors (nn) and next-nearest neighbors (nnn), and the spin variable σ, takes values of ± 1. In this form, the magnitudes of the local spin-density differences, $\langle S_z \rangle$, are subsumed into J_d and J_{se} which, more correctly, represent coupling energies. The corresponding mapping equations are of the form

$$E(M) = E^{0}_{\mathrm{Ising}} - \frac{J_d}{2}[N_{\mathrm{nn}}(\uparrow\uparrow) - N_{\mathrm{nn}}(\uparrow\downarrow)] + \frac{J_{se}}{2}[N_{\mathrm{nnn}}(\uparrow\uparrow) - N_{\mathrm{nnn}}(\uparrow\downarrow)],$$

where N_{nn} and N_{nnn} are the numbers of nn and nnn parallel ($\uparrow\uparrow$) and antiparallel spins ($\uparrow\downarrow$) in the M alignment. The coupling constants are then given by

$$J_d = \tfrac{1}{8}[E(\mathrm{AF}_1) - E(\mathrm{FM})],$$

$$J_{se} = J_d - \tfrac{1}{6}[E(\mathrm{AF}_2) - E(\mathrm{FM})]$$

in which the energies of the magnetic states are per formula unit.

C. Kanamori crystal-field Hamiltonian

As in the case of magnetic state energies, which are conveniently mapped onto an Ising spin Hamiltonian, $d \rightarrow d$ excitations can be mapped onto a crystal-field Hamiltonian, of which that proposed by Kanamori is particularly suitable.[49] For an isolated metal site, this takes the form

$$\hat{H}_{\mathrm{CF}} = \hat{H}^{0}_{\mathrm{CF}} + \frac{1}{2}\sum_{\bar{\gamma}} \sum_{\sigma} C(1,2) a^{\dagger}_{\gamma_1\sigma_1} a^{\dagger}_{\gamma_2\sigma_2} a_{\gamma_2'\sigma_2'} a_{\gamma_1'\sigma_1'}$$

in which $\bar{\gamma} = \gamma_1\gamma_2\gamma_1'\gamma_2'$ and $\bar{\sigma} = \sigma_1\sigma_2\sigma_1'\sigma_2'$. The integrals of the two-electron interactions are

$$C(1,2) = \langle \gamma_1\sigma_1, \gamma_2\sigma_2 | \frac{e^2}{\mathbf{r}_1 - \mathbf{r}_2} | \gamma_1'\sigma_1', \gamma_2'\sigma_2' \rangle,$$

where γ and γ' label the orbitals of the d manifold, and σ and σ' the electron spin. The single-particle creation and annihilation operators follow the usual notation. Three distinct types of d-d interaction can be identified.

(i) Intraband Coulomb terms $U = \langle \gamma\sigma, \gamma\sigma' \| \gamma\sigma, \gamma\sigma' \rangle$ with $\sigma \neq \sigma'$.

(ii) Interband Coulomb terms $U' = \langle \gamma\sigma, \gamma'\sigma' \| \gamma\sigma, \gamma'\sigma' \rangle$ with $\gamma \neq \gamma'$.

(iii) Interband exchange terms $J = \langle \gamma\sigma, \gamma'\sigma' \| \gamma'\sigma, \gamma\sigma' \rangle$ with $\gamma \neq \gamma'$.

TABLE I. Interband Coulomb and exchange integrals, U' and J, as a function of d orbitals, γ and γ', expressed in terms of the Racah, A, B, and C parameters.

γ	γ'	U'	J
xy, yz, xz	xy, yz, xz	$A-2B+C$	$3B+C$
x^2-y^2, z^2	x^2-y^2, z^2	$A-4B+C$	$4B+C$
xy	x^2-y^2	$A+4B+C$	C
xy	z^2	$A-4B+C$	$4B+C$
yz, xz	x^2-y^2	$A-2B+C$	$3B+C$
yz, xz	z^2	$A+2B+C$	$B+C$

These can be written in terms of the Racah A, B, and C parameters of atomic spectroscopy,[50] with $U=A+4B+3C$. U' and J on the other hand are orbital dependent, as shown in Table I, but may be conveniently averaged over the d manifold for the purposes of simplification, leading to the orbital (γ) and spin (σ) independent expressions

$$U'=A-B+C, \quad J=\tfrac{5}{2}B+C.$$

Mapping the ground and spin-allowed $d\rightarrow d$ excited states onto H_{CF}, respecting the orbital dependence of the interactions presented in Table I, gives

$$E_{\mathrm{ground}}=E^0_{\mathrm{CF}}+3A-15B,$$

$$E_{xy\rightarrow z^2}=E^0_{\mathrm{CF}}+3A-3B+\Delta_{\mathrm{CF}},$$

$$E_{xy\rightarrow x^2-y^2}=E^0_{\mathrm{CF}}+3A-15B+\Delta_{\mathrm{CF}}$$

$$E_{xz,yz\rightarrow z^2,x^2-y^2}=E^0_{\mathrm{CF}}+3A-12B+2\Delta_{\mathrm{CF}}.$$

The Laporte and spin-forbidden $xy(\uparrow)\rightarrow xy(\downarrow)$ excitation can also be mapped onto H_{CF} yielding

$$E_{xy(\uparrow)\rightarrow xy(\downarrow)}=E^0_{\mathrm{CF}}+3A-9B+2C,$$

where Δ_{CF} is the e_g-t_{2g} crystal-field splitting. Thus, the excitation energies derived from transitions between the above states can be equated directly to first-principles total-energy differences. Clearly, Δ_{CF} is obtained directly from $\Delta E_{xy\rightarrow x^2-y^2}$ while B can be derived from either of the two other Laporte forbidden, but spin-allowed transitions. In this way, the validity of mapping first-principles calculations onto the Kanamori crystal-field Hamiltonian can also be verified by comparing the first-principles total-energy difference for the spin-allowed two-electron excitation, $(xz,yz)\rightarrow(z^2,x^2-y^2)$, with that derived from Δ_{CF} and B obtained from the two spin-allowed one-electron excitations. Clearly, B can also be derived from $\Delta E_{xy,yz\rightarrow z^2,x^2-y^2}$, and this is used to predict the energy for the $xy\rightarrow z^2$ excitation. The C parameter may be obtained only from the spin-forbidden excitation $\Delta E_{xy(\uparrow)\rightarrow xy(\downarrow)}$.

D. Computational conditions

First-principles, spin polarized, periodic Hartree-Fock and density-functional theory based on localized atomic orbitals have been embodied within the CRYSTAL98 code.[51] In this study the crystal orbitals were expanded in a set of 39 atomic orbitals, 25 for V and 14 for O. In the notation used previously,[29,51] the V orbitals comprised seven shells of the type $1s(8)$, $2sp(6)$, $3sp(4)$, $4sp(1)$, $5sp(1)$, $3d(4)$, $4d(1)$ and the O orbitals four shells of the type $1s(8)$, $2sp(6)$, $3sp(4)$, $4sp(1)$, where the numbers 1,2,3,... identify the different shells and the numbers in brackets are the numbers of primitive Gaussian-type functions in the contraction for the atomic orbital. Open shell systems were treated by the UHF procedure. The inclusion of a second d shell, $4d(1)$, in the previous V basis set,[29] and subsequent reoptimization of all cation and anion valence exponents, decreased the Mulliken charge by $0.14e$ and led to energy differences between magnetic states that differed from previous values[29] by $\leqslant 10$ meV per atom. However, since this compares with typical magnetic interactions within the first-row transition-metal oxides, the V($4d$) shell and necessary valence reoptimizations were retained in all subsequent calculations. The number and angular symmetry of the Gaussian functions used here are broadly similar to those employed recently by Moreira, Illas, and Martin in their hybrid DFT study of NiO.[43]

The implementation of DFT in the CRYSTAL98 code requires the specification of an auxiliary basis of Gaussian-type functions for the fitting of the exchange-correlation potential. For this purpose, the following even-tempered bases of Gaussian-type functions were employed: 14 s-type functions with exponents in the range 0.07–4000.0, one p-type, one d-type, and one f-type function, each with exponent 0.5 were used for O, and 13 s-type functions with exponents in the range 0.1–4000.0, one p-type function with exponents in the range 0.3–0.9, one f-type function with exponent 0.8, and three g-type functions with exponents in the range 0.45–3.3 for V.

A Monkhorst-Pack shrinking factor of 8, which was used for cells of all sizes, and truncation thresholds of 10^{-7}, 10^{-7}, 10^{-7}, 10^{-7}, and 10^{-14} for the Coulomb and exchange series[51] ensured convergence of the total UHF energies of three magnetic states to $\leqslant 0.1$ meV, while self-consistent field convergence thresholds were set to 10^{-7} a.u. for both eigenvalues and total energies. These tolerances are similar to those used for a wide range of previous calculations.[32,43]

Four different types of magnetic order were considered in this study, the FM and three AF. The latter comprise the type-I (AF_1) structure, in which the double nonmagnetic primitive cell consists of ferromagnetic (100) planes of alternating spin along the [100] axis, the type-II (AF_2) structure, in which the double primitive cell consists of ferromagnetic (111) planes of alternating spin in the [111] direction, and the type-III (AF_3) structure, in which the quadruple primitive cell consists of ferromagnetic (210) planes of alternating spin in the normal direction. The Miller indices and crystal directions noted above are for the conventional crystallographic cell. The total energy and properties of the FM state can, of course, be calculated from the primitive cell, but in the present work was always extracted from the double cell. This ensures that the restriction to FM order implicit in the primitive cell does not affect the energy of the state. As a test of the various numerical parameters used in this study, the en-

TABLE II. Lattice constant a_0 (Å), total Mulliken charges $q_M(e)$, cation spin moment $n_S(\mu_B)$, and energy ΔE_M (meV/molecule) of the FM and AF_2 alignments relative to AF_1 as a function of F_0.

	a_0			q_M			n_S			ΔE_M	
F_0	AF_1	AF_2	FM	AF_1	AF_2	FM	AF_1	AF_2	FM	AF_2[a]	FM[b]
UHF	4.4545	4.4539	4.4715	1.686	1.686	1.689	3.008	3.027	3.010	10.1, 10.1	88.6, 86.9
1.0	4.3511	4.3528	4.3767	1.647	1.647	1.647	2.967	2.983	2.988	15.8, 15.8	118.4, 115.9
0.8	4.3595	4.3615	4.3865	1.608	1.607	1.611	2.959	2.976	2.986	18.4, 17.9	140.3, 135.3
0.6	4.3692	4.3737	4.4049	1.562	1.560	1.566	2.945	2.965	2.984	21.4, 20.5	169.2, 161.3
0.4	4.3761	4.3815	4.4168	1.504	1.503	1.510	2.919	2.943	2.981	26.1, 24.9	213.4, 201.4
0.2	4.3813	4.3824	4.4311	1.433	1.431	1.442	2.860	2.891	2.978	31.1, 30.4	285.0, 269.3
0.1	4.3803	4.3898	4.4577[c]	1.390	1.387	1.400	2.794	2.831	2.938	35.8, 32.4	354.4, 324.2
0.0	4.3601[c]			1.320			2.446				

[a]First entry=$[E(AF_2)-E(AF_1)$ at $a_0(AF_1)]$. Second entry=$[E(AF_2)$ at $a_0(AF_2)]-[E(AF_1)$ at $a_0(AF_1)]$.
[b]FM, as for AF_2 above.
[c]Conducting state.

ergy of the FM state was calculated by the UHF method for the primitive, double, and quadruple cells with the broken metal sublattice symmetries appropriate to the description of the various AF states. In each case, the total energy per formula unit was found to be identical to within the tolerance of the SCF convergence.

Mulliken population analyses of the crystalline orbitals were used to extract the net atomic charges, magnetic moments, and individual orbital occupations as in previous studies.

III. RESULTS AND DISCUSSION

A. Bulk lattice and electronic structure

For the entire range of hybrid Hamiltonians, the ground electronic states of the FM, AF_1, and AF_2 spin alignments were found to be insulating, with the exception of the FM alignment at $F_0=0.1$ and the pure DFT AF_1 alignment, which were found to be conducting. Lattice constants (a_0) were obtained from fourth-order polynomials fitted to total-energy-volume curves calculated within $\pm 10\%$ of the previous UHF value for the FM state (4.460 Å). The resulting a_0 for the full range of exchange-correlation potentials are given in the first three columns of Table II and shown graphically in Fig. 1. For the pure DFT description, convergence was problematic for all three magnetic structures, even with enhanced reciprocal space sampling and with Fermi smearing of the Kohn-Sham orbital occupancies. At this limit of zero exact exchange only the AF_1 alignment produced an energy-volume curve which was sufficiently smooth to yield a_0 to an acceptable accuracy. As evident in Fig. 1, the largest changes in a_0 result from the addition of correlation to exact exchange (UHF), at which point the lattice contracts by $\sim 2.4\%$ of the uncorrelated value with a slight increase in the differences between the three magnetic states. Thereafter, decreasing the amount of exact exchange leads to an increase in the AF_1 and AF_2 lattice constants to a maximum of $\sim 0.7\%$ above the correlated UHF values for $0.1 \leqslant F_0 \leqslant 0.2$. In contrast, the FM lattice constant shows no turning point at low F_0 and expands to a maximum of $\sim 1.9\%$ above the correlated UHF value. In the limit of zero exact exchange, the AF_1 lattice constant is seen to decrease sharply, the most likely cause of which is the onset of metallic behavior. A possible explanation of this abrupt change is discussed later in this section in terms of the calculated density of states.

The equilibrium bulk modulus K_0 was obtained for each Hamiltonian by a least-squares fitting of the AF_1 energy-volume data to the Murnaghan equation of state.[52] For this purpose, a restricted set of lattice constants within $\pm 2\%$ of the appropriate a_0 were used. The variation of K_0 with exchange-correlation functional is shown in Fig. 2, where it is seen to range from ~ 175 GPa for $F_0=0.1$ to ~ 200 GPa for correlated UHF. The pure UHF value is ~ 170 GPa and pure DFT (metallic) 162 GPa. While there are no experimental data, K_0 reported here might usefully be compared with values ranging from 120 GPa for CaO[53] to 190 GPa for NiO.[54] It should be noted that the Murnaghan and polynomial fits of the energy-volume data yield essentially identical optimized lattice parameters.

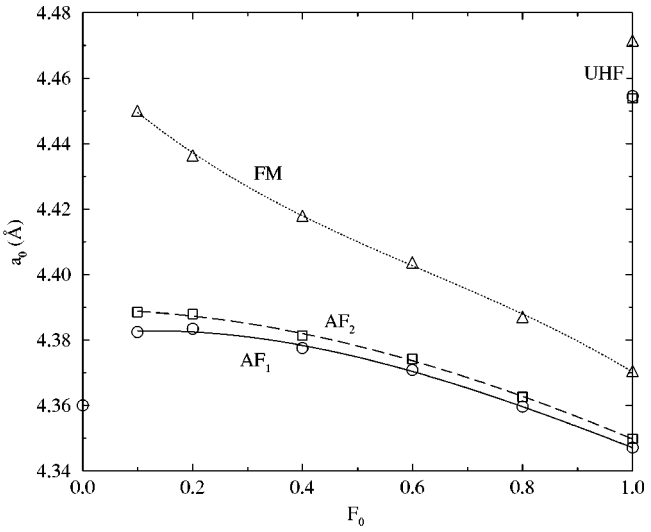

FIG. 1. The AF_1 (○), AF_2 (□), and FM (△) optimized lattice constants, a_0, as a function of F_0.

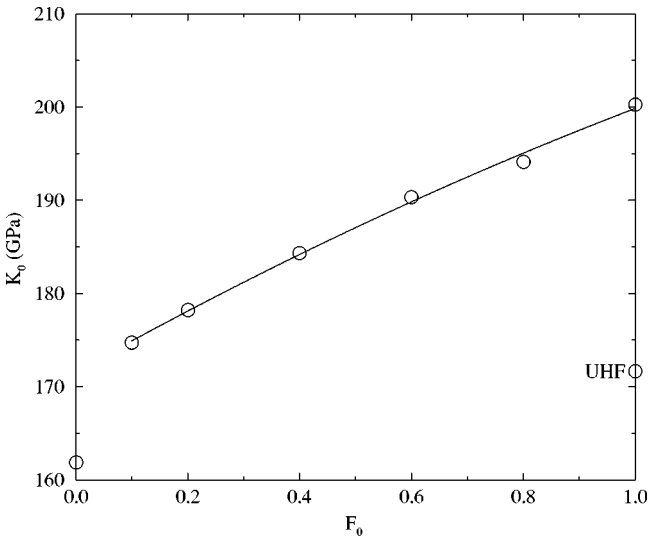

FIG. 2. The bulk modulus K_0 of the AF_1 ground state as a function of F_0.

Identical calculations for the lowest-energy spin alignment of MnO (AF_2) reveal this to be insulating across the complete range of F_0, with very similar trends to those found for VO. As shown, in Fig. 3, the addition of correlation to exact exchange contracts the lattice by $\sim 2.3\%$, while decreasing the amount of exact exchange leads to an expansion of the lattice to a maximum of $\sim 1.3\%$ above the correlated UHF value at $F_0 = 0.1$. However, a noticeable difference from VO is that there is no abrupt decrease in volume at the DFT limit. Now the experimental low-temperature lattice constant of MnO is 4.445 Å,[55] which from Fig. 3 corresponds to a value of F_0 close to 0.7. A similar exchange-correlation potential for the AF_1 alignment of VO suggests a lattice constant in the region of 4.37 Å. Figure 4 shows that the bulk modulus increases from the pure DFT value of 161 to 194 GPa for correlated UHF, with the pure UHF value

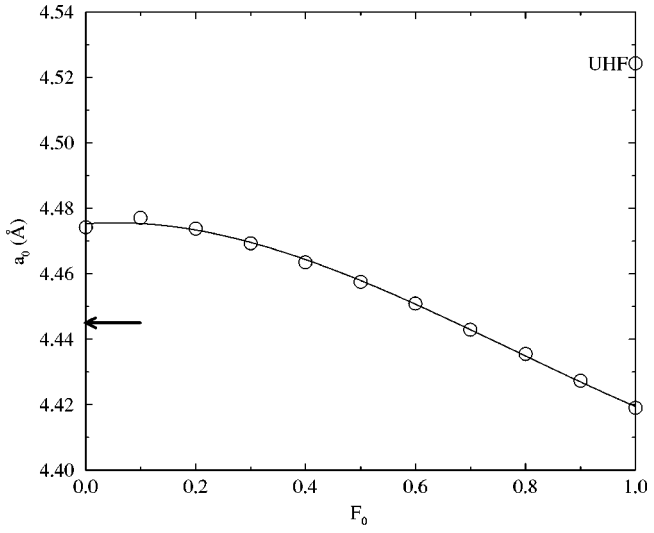

FIG. 3. The optimized lattice constant a_0 for the AF_2 ground state of MnO as a function of F_0. (The arrow marks experimental value [55]).

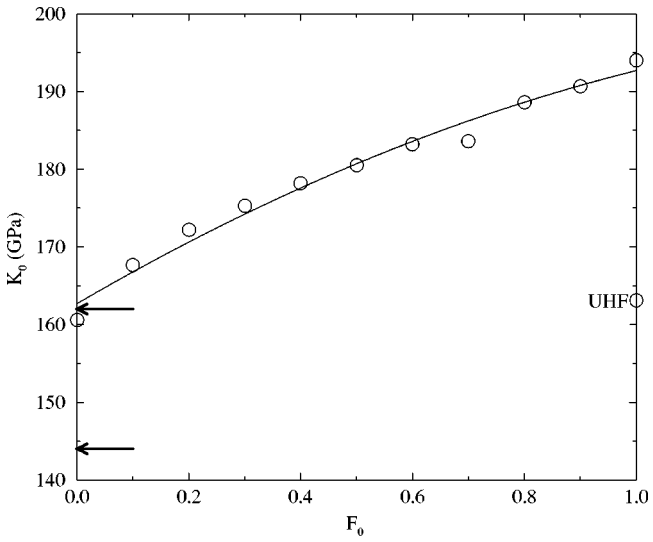

FIG. 4. The bulk modulus K_0 of the AF_2 ground state of MnO as a function of F_0. (The arrows mark the range of experimental data [55–59]).

~ 30 GPa below this, as in the case of VO. These values compare with static and dynamic experimental bulk moduli in the range 144–162 GPa.[55–59] Unlike VO, but in keeping with the variation of lattice constant, there is no abrupt decrease in bulk modulus of MnO in the DFT limit. Thus, the differences between the two materials in the purely local functional might reasonably be attributed to the transition to a metallic ground state in VO and the retention of an energy gap in MnO.

Turning now to the electronic structure, the Mulliken charges and cation spin moments for VO shown in Table II indicate a largely ionic system for $F_0 \geqslant 0.6$. Both the ionicity and local cation moment decrease as the proportion of exact exchange decreases. This implies that the gross electronic state of the crystal tends not toward singly charged ions, which would require an increase in the cation spin moment, but instead toward a metallic solution. An interesting observation here is that the spin polarization of the oxygen sublattice varies both with F_0 and magnetic order. Typical values for the net spin densities on the two oxygen atoms of the magnetic unit cell are $(-0.007, 0.004)$ and $(0.012, 0.012)$ for the AF_1 and FM alignments, respectively, at the limit of correlated exact exchange and $(-0.010, 0.007)$ and $(0.024, 0.024)$ for an F_0 value of 0.1. Spin polarization of the anion is forbidden by symmetry in the AF_2 alignment. Such polarization of the anion in the FM state has been noted in DFT studies of NiO (Ref. 43) but has no basis in experimental observation. The decreased ionicity of the FM state based on exact exchange derived from the present, enriched V basis set compared with that reported previously[29] can be attributed, in part, simply to the inclusion of a $4d$ polarization function and, in part, to the optimization of the orbital exponent. To show this, an unoptimized V^{2+} bare ion $4d$ shell was added to the 6-shell V basis of the previous study, leading to a decrease in the ionicity of the FM state by $0.05e$, without any change in the valence orbital exponents.

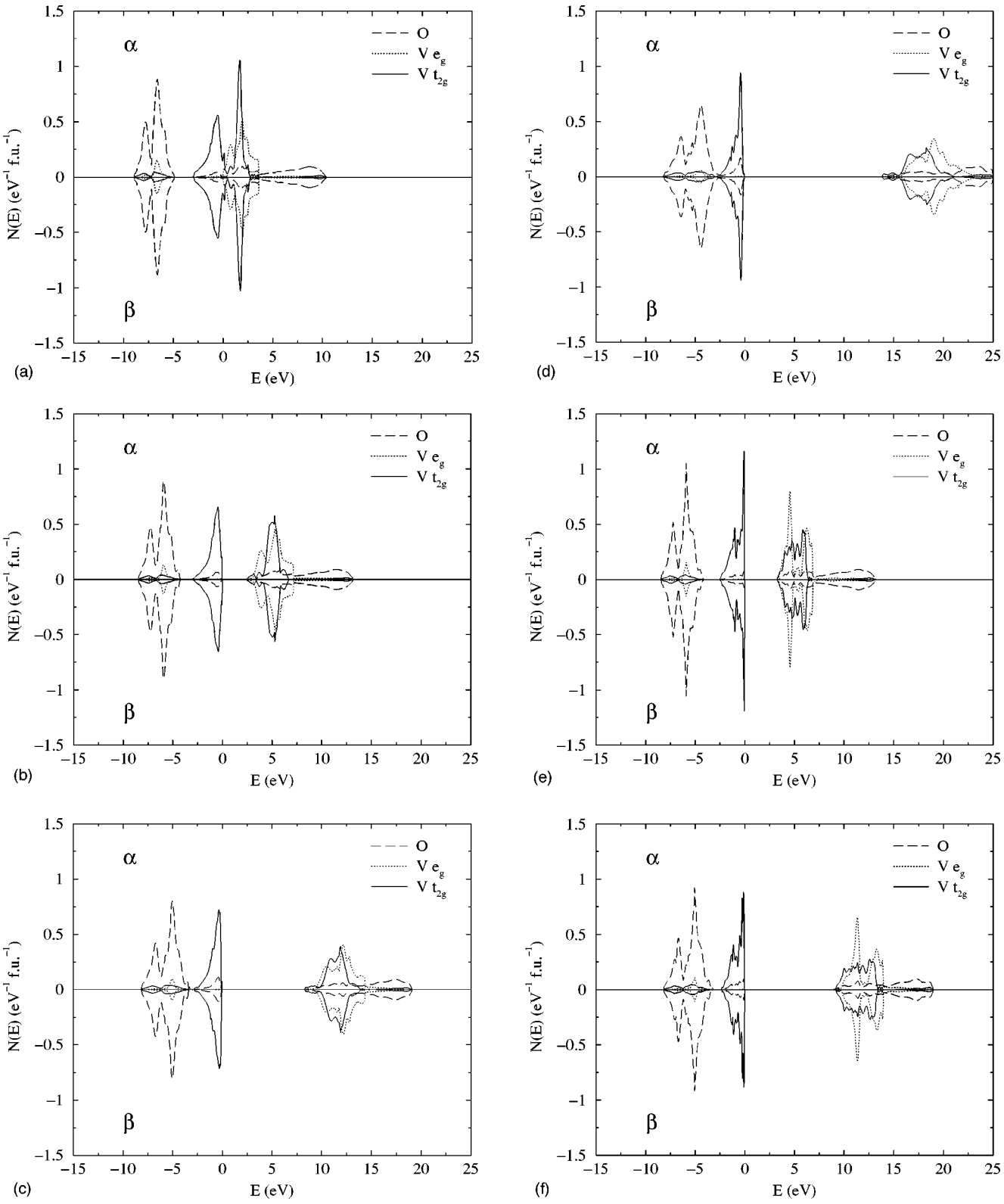

FIG. 5. Orbital projected densities of states $N(E)$ vs energy E; for the AF_1 state (a) $F_0=0.0$, (b) $F_0=0.2$, (c) $F_0=0.6$, (d) $F_0=1.0$; for the AF_2 state (e) $F_0=0.2$, (f) $F_0=0.6$, (g) $F_0=1.0$; for the FM state (h) $F_0=0.2$, (i) $F_0=0.6$, (j) $F_0=1.0$. Fermi energies are set to zero.

The energies of the AF_2 and FM alignments relative to AF_1 given in Table II show that AF_1 order is lowest in energy for the entire range of exchange-correlation functionals considered in this study. This is in keeping with the largely high spin t_{2g}^3 d-orbital occupation and cation moments revealed by the Mulliken analyses. In the rocksalt transition-metal oxides, the strength of the superexchange interaction depends critically on the occupation of the e_g orbitals, for it

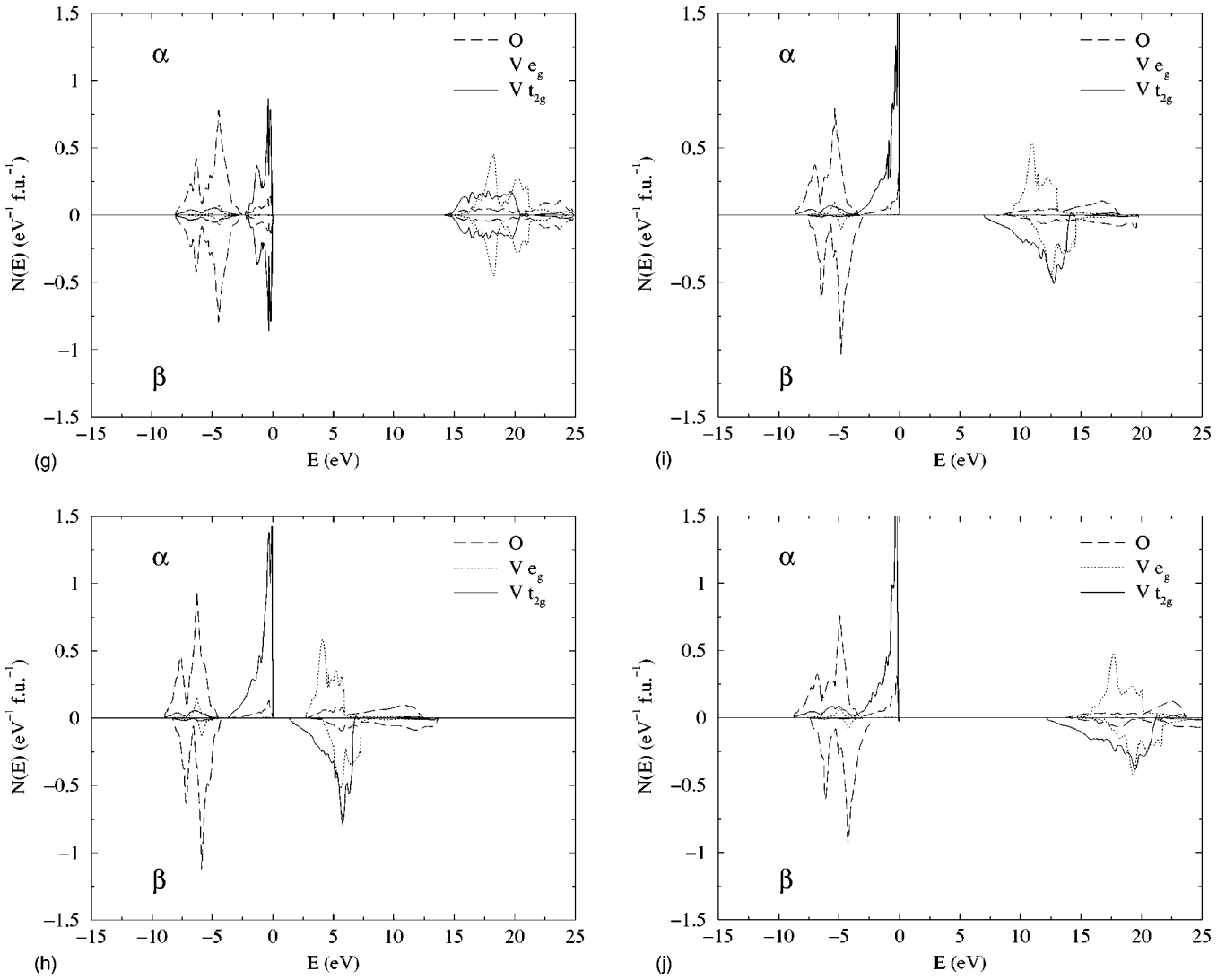

FIG. 5. (*Continued*.)

is these that strongly overlap the $2p$ orbitals of the neighboring anions. The superexchange dominated AF_2 ground state found in MnO and NiO would not therefore be expected in this material. The dependence of a_0 on magnetic order is indicative of a strong spin-lattice interaction in VO, and to gauge the strength of this coupling, identical calculations in the limit of exact exchange were carried out for MnO. Lattice parameters of 4.423, 4.419, and 4.425 Å were obtained for the AF_1, AF_2 (ground-state), and FM symmetries, respectively, leading to a maximum variation of 0.006 Å, or 0.136% between the AF_2 and FM values. This compares with a maximum variation of 0.026 Å, or 0.598% between the AF_1 and FM states in VO, which is approximately four times that in MnO.

Figure 5 contains the atomic-orbital projected densities of states (DOS) for the three magnetic states, for 20%, 60%, and 100% exact exchange, all at the AF_1 lattice parameter. Also shown is the DOS for the metallic AF_1 state derived from the pure DFT potential. Details of the energy gaps and valence bandwidths extracted from these plots are given in Table III. The filled to unfilled band gap for each of the magnetic states is found to vary linearly with F_0, as shown in Fig. 6, with

$$\Delta E_g(\mathrm{FM}) < \Delta E_g(\mathrm{AF}_1) < \Delta E_g(\mathrm{AF}_2),$$

for the entire range of exchange-correlation potentials. They range from ~ 14 eV at the correlated UHF limit down to ~ 0.9 eV at the AF_1 stability limit of 10% exact exchange. [In the interests of clarity the (wide) UHF gaps have been omitted from Fig. 6.] An extension of the lines of best fit down to $F_0 = 0.0$ for the AF_2 and FM states suggests that the former may retain a small gap of perhaps (0.3–0.5) eV, whereas the latter will almost certainly be metallic. The DOS shown in Fig. 5 indicate that for *all* insulating phases the filled to unfilled gaps are spanned by vanadium states, leading to an unambiguous classification of VO as a MH insulator. Furthermore, the character of the valence- and conduction-band edges is seen to be independent of magnetic order, so that pressure or temperature induced magnetic transitions would not be expected to result in any change of the

TABLE III. Filled to unfilled gap ΔE_g (eV) and filled O($2p$) and V(t_{2g}) bandwidths, W_O (eV) and $W_{t_{2g}}$ (eV) for the AF_1 alignment as a function of F_0.

	ΔE_g			AF_1	AF_2	FM
F_0	AF_1	AF_2	FM	W_O, $W_{t_{2g}}$	W_O, $W_{t_{2g}}$	W_O, $W_{t_{2g}}$
UHF	13.955	14.039	13.153	7.297[a]	7.114[a]	7.899[a]
1.0	13.805	14.142	12.141	8.269[a]	5.537, 2.275	8.736[a]
0.8	11.045	11.500	9.543	8.254[a]	5.278, 2.335	8.696[a]
0.6	8.242	8.896	6.935	5.053, 3.121	4.978, 2.340	8.638[a]
0.4	5.416	6.196	4.203	4.681, 3.014	4.677, 2.424	8.737[a]
0.2	2.445	3.239	1.358	4.343, 3.034	4.303, 2.521	4.731, 3.710
0.1	0.926	1.756	0.000	4.178, 3.087	4.104, 2.613	4.478, 3.748
0.0	0.000			4.046, 13.718[b]		

[a]Where the O($2p$) and V(t_{2g}) bands overlap, the total valence bandwidth is presented as a single entry.
[b]Where the filled V(t_{2g}) band and empty bands overlap, the O($2p$) and net conduction bandwidths are both presented.

insulating character of nondefective VO. An orbital projection of the V($3d$) bands confirms that AF_1 symmetry splits the twofold O_h degeneracy of the $3d$ states in the FM/nonmagnetic lattice into four nondegenerate subbands, leading to an overall d-level ordering and occupancy of the form

$$\underbrace{d^1_{xz}(\uparrow)/d^1_{yz}(\uparrow) < d^1_{xy}(\uparrow)}_{\text{filled}} < \underbrace{d^0_{xy}(\downarrow) < d^0_{xz}(\downarrow)/d^0_{yz}(\downarrow) < d^0_{z^2}(\uparrow) < d^0_{x^2-y^2}(\uparrow)\cdots}_{\text{empty}}.$$

(Again, in the interests of visual clarity, this set of more detailed projections is not shown on the DOS plots.) As F_0 decreases from 0.6 to 0.1, a gap opens between the filled V(t_{2g}) bands, which broadens by $\sim$0.13 eV, and the O($2p$) bands, which narrows by $\sim$0.88 eV. More importantly, despite an increase in the weight of the minority V(e_g) states as the percentage of exact exchange is reduced, the lower edge of the conduction band in the AF_1 alignment remains predominantly of t_{2g} character for the entire range of single-particle potentials we have considered.

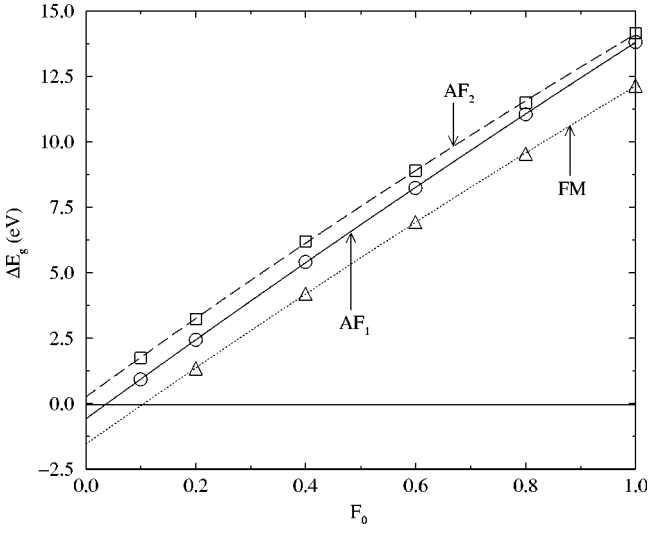

FIG. 6. Filled to unfilled energy gap ΔE_g for the AF_1 (○), AF_2 (□), and FM (△) states as a function of F_0.

These observations raise some interesting issues. While all the low energy gap excitations are locally Laporte forbidden ($\Delta\ell = 0$), as they must be for a MH system, the lowest of these, $d_{xy}(\uparrow) \rightarrow d_{xy}(\downarrow)$, is also spin forbidden ($\Delta S \neq 0$). It is unlikely, therefore, that the latter could be identified with any measurable adsorption edge. For the B3LYP potential, which has been observed to yield anion to cation gaps in impressive agreement with data from a variety of sources,[48] the edge to edge $d_{xy}(\uparrow) \rightarrow d_{xy}(\downarrow)$ ($\Delta S \neq 0$) gap in AF_1 VO is $\sim$2.5 eV, the spin-allowed $d_{xy}(\uparrow) \rightarrow d_{z^2}(\uparrow)$ gap $\sim$3.0 eV, and the V$\rightarrow$O charge-transfer gap $\sim$3.5 eV, and it is the latter that might reasonably be expected to lead to an (strong) absorption edge. For interest, we have also calculated the electronic structure of nondefective VO based on the B3LYP potential, but at the observed lattice constant for the stoichiometric, *defective* material, 4.063 Å.[8] These calculations indicate the continued stability of the AF_1 magnetic state, and the existence of a $d_{xy}(\uparrow) \rightarrow d_{xy}(\downarrow)$ gap of width 0.97 eV. While this is substantially lower than for the equilibrium structure, the system remains assuredly insulating. Our calculations suggest, therefore, that the metallicity observed in samples of VO_x of varying stoichiometry should not be attributed to the properties of the underlying perfect lattice at the contracted cell dimensions, but is more likely a consequence of the presence of defects.

This description of the band structure is reflected in Mulliken analyses of the total wave function. At the UHF level of approximation, the overlap population between nearest-neighbor V and O sites is $-0.04e$, that between V($\uparrow$) and V($\downarrow$) sites $0.006e$, and there is virtually no overlap density between V sites with the same spin. The overlap population between O sites is $-0.008e$, which is marginally antibonding, leading to an overall UHF description of the AF_1 spin alignment as essentially ionic. The introduction of correlation into the UHF potential leads to a general increase in

bond populations, indicating a slight overall decrease in the degree of ionicity. Reducing the proportion of exact exchange results in further changes to the overlap populations in AF_1 VO, with an increase in bonding between all nearest-neighbor V sites and a reduction in the antibonding character of both V-O and O-O interactions. Progression to the metallic state in the DFT limit leaves the latter two interactions virtually unchanged, whereas the populations associated with V(↑)-V(↓) and V(↑)-V(↑) nn pairing increase dramatically from $0.022e$ and $0.002e$, respectively, at $F_0=0.1$ to $0.030e$ and $0.016e$, with a lowering of the Fermi level within the t_{2g} manifold. Thus in the pure DFT description of VO it is likely that the metallic state arises from an increased overlap of nearest-neighbor V($3d$) orbitals..

Overall, the electronic structure of the AF_2 state revealed by the DOS is quite similar to that of the AF_1, with only minor changes resulting from the difference in symmetry. In contrast to the AF_1 alignment, no splitting of the V(e_g) and V(t_{2g}) states beyond that produced by the octahedral crystal field is observed, which is entirely consistent with the different symmetries of the two magnetic supercells. Decreasing the proportion of exact exchange leads to an increasing separation of the valence O($2p$) and V(t_{2g}) bands, as in the case of the AF_1 alignment. While the O($2p$) bandwidths are similar, the V(t_{2g}) bands are narrower, indicating a more restricted overlap of orbitals than in the AF_1 alignment. The reason for this is the different number of nn cations with parallel and antiparallel spins in the two alignments. In AF_1 symmetry, each cation interacts with four parallel and eight antiparallel metal spins, whereas in AF_2 symmetry, the interactions are with six parallel and six antiparallel spins. Overlap of the occupied d states is thus more strongly inhibited by exchange in the latter magnetic structure, leading to a narrower d band. This mechanism has no effect on the anion p band, which is almost identical for both types of antiferromagnetism. The O($2p$) band narrows by ~ 1.4 eV as F_0 varies from 1.0 to 0.1, whereas the V(t_{2g}) band broadens by ~ 0.3 eV across the same range. As in the AF_1 alignment, the conduction-band edge is dominated by minority spin t_{2g} states with an increasing weighting of the e_g states as F_0 is decreased.

The DOS of the FM states are naturally quite different to those derived from antiferromagnetic order. The net spin polarization carried by the lattice acts to suppress the energy of the majority-spin orbitals relative to the corresponding minority-spin orbitals, leading to broader bands. As shown in Fig. 5, only majority-spin V(t_{2g}) orbitals occupy the valence-band edge, while the conduction-band edge is formed from minority-spin V(e_g) orbitals. As a result of the band broadening, a splitting of the O($2p$) and V($t2g$) valence bands does not occur until the exact exchange falls below 20%.

B. Magnetism and phase transitions

Direct and superexchange coupling energies extracted from the total energies of the FM, AF_1, and AF_2 spin alignments, as outlined in Sec. II A, are given in Table IV. From the sign of J_d and J_{se} it is evident that both direct and superexchange interactions favor antiferromagnetic alignment of both nn and nnn vanadium spins. There is a fourfold increase in the magnitude of J_d and J_{se} over the range of single-particle potentials we have considered and, as expected from arguments presented in Sec. III A, direct exchange is found to be more than five times stronger than superexchange. It is straightforward to show that for an Ising spin Hamiltonian of the type invoked in this study, the difference in energy between the AF_1 and AF_3 alignments, $[E(AF_1)-E(AF_3)]$, is $2J_{se}$, in which case the mapping we have used here leads to a *lower* energy for AF_3 than AF_1. For the value of J_{se} *derived* from UHF energies, for example, the difference is $+4$ meV, whereas the *direct total-energy difference* is -27.5 meV. Thus for fully stoichiometric, nondefective VO the stability of the lowest-energy spin alignments derived from a mapping of E(FM), $E(AF_1)$, and $E(AF_2)$ onto H_{Ising} is predicted to be in the order

$$AF_3 > AF_1 > AF_2 > FM,$$

in contrast to the order of stability obtained *directly* from first-principles calculations, which is

$$AF_1 > AF_2 > AF_3 > FM.$$

The root of the disparity lies in the assumption, which is implicit in all mappings of this sort, that the electronic structures and bonding in the four magnetic phases are essentially identical. Differences in energy between them are posited to arise solely from the direct and superexchange coupling of identical local moments in identical electronic environments, leading to identical coupling constants/energies. While this assumption seems to hold for the more ionic systems, MnO and NiO,[60] it patently does not hold in the case of VO, as shown by the strong spin-lattice interaction discussed in Sec. II A. Further evidence for the small, but important differences between the three antiferromagnetic phases is found in the integrated densities of valence states. For example, the total UHF oxygen populations (per formula unit) in the AF_1, AF_2, and AF_3 alignments are $5.97e$, $5.92e$, and $5.44e$, respectively, and corresponding vanadium populations $2.99e$, $3.00e$, and $2.95e$. Thus, the population of the O($2p$) band in AF_3 alignment is $\sim 0.5e$ less than in the two other AF phases

TABLE IV. The direct, J_d (meV), and superexchange, J_{se} (meV), coupling constants and mean-field transition temperatures T_N (K) for the AF_1 and AF_3 alignments at the optimized AF_1 lattice constants, all as a function of F_0.

F_0	J_d	J_{se}	T_N (AF_1)	T_N (AF_3)
UHF	−11.08	+2.02	186.86	233.65
1.0	−14.80	+2.30	263.20	316.65
0.8	−17.54	+2.79	309.87	374.51
0.6	−21.15	+3.50	369.15	450.14
0.4	−26.67	+4.55	460.45	565.97
0.2	−35.62	+6.69	593.49	748.79
0.1	−44.31	+8.80	721.67	925.83

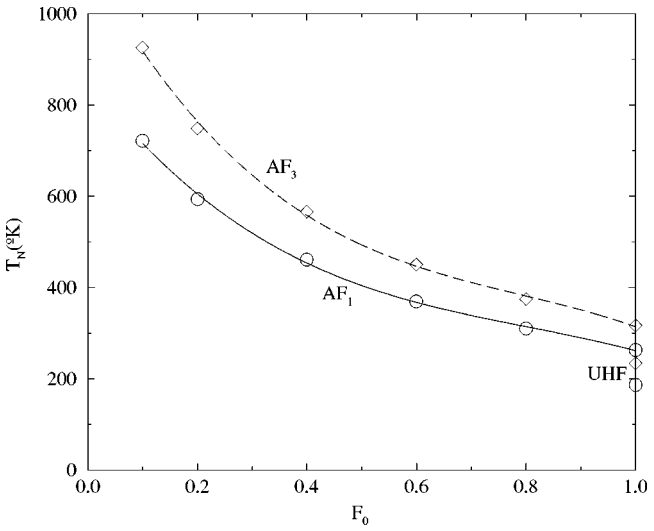

FIG. 7. Mean-field critical temperature for the AF_1 (○) and AF_3 (◇) magnetic states as a function of F_0.

and it is precisely these differences that invalidate the assumptions implicit in mapping first-principles energies onto H_{Ising} in the case of VO.

The above remarks notwithstanding, we have used J_d and J_{se} to provide qualitative estimates of the Néel temperatures of the AF_1 and AF_3 phases. Elementary considerations indicate that within a mean-field approximation for H_{Ising}, $\langle\sigma\rangle$ for these two phases is given by

$$\langle\sigma\rangle_{\mathrm{AF}_1}=\tanh\left[-\frac{2J_d+3J_{se}}{k_BT}\right],$$

$$\langle\sigma\rangle_{\mathrm{AF}_3}=\tanh\left[-\frac{2J_d+J_{se}}{k_BT}\right],$$

which as $\langle\sigma\rangle\to 0$ leads to

$$T_N[\mathrm{AF}_1]=\frac{-2J_d-3J_{se}}{k_B},$$

$$T_N[\mathrm{AF}_3]=\frac{-2J_d-J_{se}}{k_B}.$$

The variation of T_N with F_0 is shown in Fig. 7, where it should be noted that mean-field theory is known to overestimate T_N by a factor $\sim 4/3$ through the neglect of fluctuations. Recent work on MnO and NiO[61] has shown that direct and superexchange coupling constants close to the magnon derived values are obtained from hybrid functionals containing 20%–50% exact exchange, which for VO would lead to an AF_1 critical temperature in the range 300–450 K.

C. Crystal-field excitations

The existence of weak, orbitally forbidden ($\Delta l=0$) excitations in the paradigm magnetic insulators NiO and MnO has been revealed by optical-absorption studies and electron energy-loss spectroscopy. The absorptions are found to lie within the bulk band gap, and have been attributed to $d\to d$ transitions on the basis of first-principles multireference cluster calculations.[62–64] It is well known that such excitations are strongly localized, with the characteristics of Frenkel excitons.[65] In previous studies of NiO, $d\to d$ excited states were found to be stable both in the bulk and the reduced symmetries of the inner and outer layers of {100} slabs, with differences in transition energy of <0.05 eV for identical O_h crystal-field excitations in the two geometries.[66] In the present work, stable excited states could not be obtained in the bulk, for reasons that remain unclear, so that all the calculations reported here refer to the central plane of {100} slabs consisting of three and five layers. As before,[66] the slabs were constructed from (surface) 2×2 supercells in which the $d\to d$ excitation is confined to one vanadium atom per supercell of the central plane where the (local) crystal field is identical to the bulk and of O_h symmetry. The reference system we used has the z^2 orbital perpendicular to the basal {100} slab planes, with the (x^2-y^2) orbital pointing toward the neighboring oxygen atoms. It is important to emphasize that the energies of the excited states were obtained by variational minimization of the total (excited-state) energy. That is to say, the total energy of the excited state, which is a *local minimum* in the energy hyperspace of the system, is found directly by an identical, variational procedure to that for the ground state. This leads to excitation energies which are simple *direct* differences between ground and excited-state total energies.

Now the expressions for the crystal-field state energies given in Sec. II C, strictly speaking, hold for an isolated d^n ion, so that they are appropriate for a free ion or an isolated impurity in a nonmagnetic lattice. However, for ordered magnetic systems, the interaction with neighboring spins must be included. In the case of VO, the magnetic states of which are dominated by the direct coupling of nn spins (J_d), the energies of the crystal-field states in the FM alignment can be written as

$$E_g=E^0_{\mathrm{CF}}+3A-15B-12J_d,$$

$$E_{xy\to z^2}=E^0_{\mathrm{CF}}+3A-3B+\Delta_{\mathrm{CF}}-8J_d,$$

$$E_{xy\to x^2-y^2}=E^0_{\mathrm{CF}}+3A-15B+\Delta_{\mathrm{CF}}-8J_d,$$

$$E_{xz,yz\to z^2,x^2-y^2}=E^0_{\mathrm{CF}}+3A-12B+2\Delta_{\mathrm{CF}}-J_d,$$

$$E_{xy(\uparrow)\to xy(\downarrow)}=E^0_{\mathrm{CF}}+3A-9B+2C-4J_d,$$

leading to the following excitation energies:

$$\Delta E_{xy\to z^2}=12B+\Delta_{\mathrm{CF}}+4J_d,$$

$$\Delta E_{xy\to x^2-y^2}=\Delta_{\mathrm{CF}}+4J_d,$$

$$\Delta E_{xz,yz\to z^2,x^2-y^2}=3B+2\Delta_{\mathrm{CF}}+8J_d,$$

$$\Delta E_{xy(\uparrow)\to xy(\downarrow)}=6B+2C+8J_d.$$

Likewise, in the AF_1 alignment, the crystal-field energies can be written as

$$E_g=E^0_{\mathrm{CF}}+3A-15B+4J_d,$$

$$E_{xy\to z^2}=E^0_{\mathrm{CF}}+3A-3B+\Delta_{\mathrm{CF}}+8J_d,$$

TABLE V. Excitation energies ΔE (eV) and excited orbital charge $(\alpha+\beta)$ and spin $(\alpha-\beta)$ occupation for the three spin-allowed, Laporte-forbidden transitions as a function of F_0.

		$xy\rightarrow z^2$			$xy\rightarrow x^2-y^2$			$xz,\ yz\rightarrow z^2,\ x^2-y^2$		
F_0	State	ΔE	$\alpha+\beta$	$\alpha-\beta$	ΔE	$\alpha+\beta$	$\alpha-\beta$	ΔE	$\alpha+\beta$	$\alpha-\beta$
UHF	FM	2.519	0.925	0.94	1.175	0.916	0.943	2.689	0.936, 0.936	0.934, 0.947
1.0	FM	2.638	0.921	0.939	1.300	0.911	0.939	2.932	0.931, 0.929	0.930, 0.942
	AF_1	2.649	0.914	0.930	1.308	0.930	0.937	3.182	0.923, 0.924	0.923, 0.939
0.9	FM	2.602	0.916	0.934	1.294	0.907	0.936	2.920	0.927, 0.925	0.925, 0.940
0.8	FM	2.563	0.910	0.929	1.285	0.901	0.932	2.905	0.923, 0.921	0.921, 0.936
0.7	FM	2.522	0.902	0.924	1.278	0.896	0.929	2.888	0.916, 0.917	0.917, 0.932
0.6	FM	2.471	0.893	0.915	1.267	0.888	0.924	2.863	0.911, 0.911	0.910, 0.926
0.5	FM	2.416	0.877	0.900	1.251	0.878	0.918	2.837	0.902, 0.904	0.902, 0.921
0.4	FM	2.338	0.847	0.868	1.233	0.867	0.908	2.798	0.890, 0.895	0.887, 0.911
0.3	FM	2.194	0.761	0.770	1.200	0.849	0.896	2.734	0.867, 0.881	0.864, 0.898
	AF_1	2.279	0.828	0.851	1.210	0.883	0.897	3.164	0.865, 0.872	0.868, 0.893

$$E_{xy\rightarrow x^2-y^2}=E^0_{\mathrm{CF}}+3A-15B+\Delta_{\mathrm{CF}}+8J_d,$$

$$E_{xz,yz\rightarrow z^2,x^2-y^2}=E^0_{\mathrm{CF}}+3A-12B+2\Delta_{\mathrm{CF}}-4J_d,$$

$$E_{xy(\uparrow)\rightarrow xy(\downarrow)}=E^0_{\mathrm{CF}}+3A-9B+2C+12J_d,$$

and the excitation energies as

$$\Delta E_{xy\rightarrow z^2}=12B+\Delta_{\mathrm{CF}}+4J_d,$$

$$\Delta E_{xy\rightarrow x^2-y^2}=\Delta_{\mathrm{CF}}+4J_d,$$

$$\Delta E_{xz,yz\rightarrow z^2,x^2-y^2}=3B+2\Delta_{\mathrm{CF}}-8J_d,$$

$$\Delta E_{xy(\uparrow)\rightarrow xy(\downarrow)}=6B+2C+8J_d.$$

From this, it is clear that within our approximation of including only J_d interactions, the energies of the three one-electron excitations are identical in the FM and AF_1 alignments, whereas there is a difference of $16J_d$ for the two-electron excitation. For this reason, the majority of calculations were performed in the computationally more convenient FM arrangement, although, as a check we have calculated excitation energies in both spin alignments for 100% and 30% exact exchange. However, the optimized AF_1 lattice constants were used throughout.

The energies of the spin-allowed $(\Delta S=0)$ one-electron $xy\rightarrow z^2$ and $xy\rightarrow x^2-y^2$, and two-electron $xz,yz\rightarrow z^2,x^2-y^2$ trilayer excitations as a function of F_0 are given in Table V and those for the spin-forbidden $xy(\uparrow)\rightarrow xy(\downarrow)$ excitation in Table VI. In both cases the $(\alpha+\beta)$ and $(\alpha-\beta)$ orbital occupancies of the excited state indicate that these excitations are highly local for the entire range of potentials. No stable excitations were found for $F_0<0.3$, so that the B3LYP potential $(F_0=0.2)$ appears to be unable to support these elementary excitations in VO. The introduction of correlation into the UHF potential increases the three spin-allowed excitation energies, and decreases the spin-forbidden energy, which is entirely reasonable, for only the latter involves spin pairing. Tables V and VI also support our inclusion of only the nn J_d interactions in the crystal-field energies. Thus for the one-electron excitations, the differences between the FM and AF_1 energies vary from 0.008 to 0.085 eV, whereas for the two-electron excitation, which in our approximation involves a difference of $16J_d$, the differences between the two alignments vary from 0.25 to 0.43 eV. As a further check on the consistency of our calculations, the values of J_d given in Table IV, which are obtained solely from the ground electronic state, predict differences of 0.24 and 0.48 eV for the two-electron excitation. Thereafter, both the energies and occupancies of all four excitations were found to decrease with decreasing exact exchange. As a check on the influence of slab thickness, UHF calculations of the spin-allowed excitations were carried out for five-layer slabs, resulting in decreases of 0.03 and 0.08 eV, respectively for the $xy\rightarrow z^2$ and $xz,\ yz\rightarrow z^2,\ x^2-y^2$ excitations, which are perpendicular to the slab, while the energy of the in-plane $xy\rightarrow x^2-y^2$ remains unchanged. Quite reasonably, perpendicular excitations are the more sensitive to slab thickness, though the relatively small differences between the three- and five-layer energies suggest that Tables V and VI give a

TABLE VI. Excitation energy ΔE (eV) and excited orbital charge and spin occupation for the spin- and Laporte-forbidden $xy(\uparrow)\rightarrow xy(\downarrow)$ transition as a function of F_0.

F_0	State	ΔE	$\alpha+\beta$	$\alpha-\beta$
UHF	FM	1.395	1.013	−0.976
1.0	FM	1.151	1.010	−0.964
	AF_1	1.133	1.015	−0.971
0.9	FM	1.072	1.012	−0.964
0.8	FM	1.012	1.012	−0.959
0.7	FM	0.950	1.011	−0.952
0.6	FM	0.881	1.011	−0.943
0.5	FM	0.809	1.009	−0.930
0.4	FM	0.724	1.005	−0.911
0.3	FM	0.619	0.997	−0.882
	AF_1	0.675	1.018	−0.905

TABLE VII. Racah B (eV) and C (eV) parameters, d-manifold averaged interband exchange constant, J (eV) and ratio $\Gamma = C/B$ for the V ion both free and within the lattice, as a function of F_0. Also shown are the crystal-field splitting parameter Δ_{CF} (eV) and the two-particle $(xz,yz) \rightarrow (z^2, x^2-y^2)$ excitation energy ΔE_{2P} (eV) and deviation from the directly calculated value (Table V) predicted on the basis of the single-particle B and Δ_{CF} parameters.

		Lattice (trilayer)						Free V^{2+} ion			
F_0	State	B	C	Δ_{CF}	J	ΔE_{2P}	Γ	B	C	J	Γ
UHF	FM	0.1119	0.4059	1.220	0.6858	2.687 (−0.09%)	3.6264	0.1143	0.4536	0.7394	3.9685
1.0	FM	0.1115	0.3003	1.359	0.5790	2.934 (+0.07%)	2.6939	0.1152	0.3534	0.6414	3.0677
	AF_1	0.1118	0.3895	1.367	0.6689	3.188 (+0.19%)	3.4853				
0.9	FM	0.1090	0.2721	1.357	0.5447	2.915 (−0.19%)	2.4965	0.1132	0.3369	0.6199	2.9761
0.8	FM	0.1064	0.2564	1.355	0.5225	2.890 (−0.52%)	2.4092	0.1113	0.3226	0.6009	2.8985
0.7	FM	0.1036	0.2415	1.356	0.5006	2.867 (−0.70%)	2.3310	0.1093	0.3131	0.5864	2.8646
0.6	FM	0.1004	0.2250	1.352	0.4759	2.835 (−1.00%)	2.2414	0.1073	0.3100	0.5783	2.8891
0.5	FM	0.0971	0.2078	1.345	0.4505	2.793 (−1.54%)	2.1401	0.1053	0.3132	0.5765	2.9744
0.4	FM	0.0921	0.1913	1.338	0.4216	2.742 (−2.03%)	2.0765	0.1033	0.3179	0.5762	3.0774
0.3	FM	0.0828	0.1819	1.321	0.3889	2.648 (−3.13%)	2.1965	0.1013	0.3248	0.5781	3.2063
	AF_1	0.0891	0.1911	1.331	0.4139	3.170 (+0.19%)	2.1443				

qualitatively correct indication of the weak absorptions in stoichiometric VO, especially in view of the relative insensitivity of the energies to the proportion of exact exchange.

In the case of NiO (Refs. 67 and 68), La_2CuO_4 (Refs. 69 and 70), and $Sr_2CuO_2Cl_2$ (Ref. 71) and other first-row transition-metal chalcoginides where $d \rightarrow d$ excitations have been observed, an important consideration is their juxtaposition to the strong anion to cation charge-transfer absorption edge. For MH systems there is the added interest of comparing the energies of on-site and edge to edge (band) excitations of the same orbital types, from which energies of Frenkel localization can be estimated. While such comparisons can be made for the full range of exchange-correlation potentials, the evidence presented in Ref. 48 suggests that comparisons for the B3LYP potential might be the most meaningful. In the absence of direct values, extrapolating the energies given in Tables V and VI yields approximate B3LYP values of ~0.5, ~2.1, and ~1.2 eV for the crystal-field $xy(\uparrow) \rightarrow xy(\downarrow)$, $xy(\uparrow) \rightarrow z^2(\uparrow)$, and $xy(\uparrow) \rightarrow x^2-y^2(\uparrow)$ excitations, respectively. These compare with edge to edge (band) values in the AF_1 alignment of ~2.5, ~3.2, and ~3.1 eV respectively, leading to Frenkel localization energies of ~2.0, ~1.1, and ~1.9 eV. Furthermore, all four crystal-field excitations are predicted to lie below the (strong) V→O charge-transfer absorption.

Values for B, C, Δ_{CF}, d-averaged J, and the Tanabe-Sugano Γ parameter (C/B)[72] derived from the trilayer excitations and free V^{2+} ion are presented in Table VII. As the proportion of exact exchange is decreased the lattice values of B, C, and J decrease, which once again reflects the increasing covalency of the bonding in VO as the limiting DFT description is approached. Since the crystal-field splitting varies inversely with the lattice parameter, it too decreases with decreasing exact exchange. For the free ion, both B and J decrease with F_0, although there appears to be a very minor upturn in J as the stability limit for the crystal-field excitations is reached. Our free ion B, C, and Γ compare with values of 0.0936, 0.4038, and 4.314 eV, respectively, reported by Tanabe and Sugano.[72] A comparison of the lattice and free-ion parameters shows that the Racah C parameter is strongly reduced by the crystalline environment, notably as the proportion of exact exchange decreases, leading to reduced Hund exchange coupling. Such a pattern is indeed noted in the later transition metal oxides, in which pure DFT-GGA (generalized gradient approximation) calculations predict the onset of low spin states at modest hydrostatic pressures.[73] However, (XES) measurements in FeO (Ref. 74) indicate that if such spin transitions do occur, they will be at significantly greater pressures than those derived from the GGA calculations. Data collected and presented by Tanabe and Sugano[72] suggest that the value of Γ for free ions, substitutional impurities, and cations in the binary oxides is roughly constant and in the range 4.2–4.5 across the first-row transition metals. Here, only the UHF values approach this range, and while the free-ion values for low F_0 might be acceptably close, in the crystalline environment, Γ is reduced to pathologically low levels as the proportion of exact exchange is reduced.

Also included in Table VII is a comparison of $\Delta E_{xy,yz \rightarrow z^2,x^2-y^2}$ derived from the (mapped) crystal-field parameters and those obtained directly from first-principles calculations. The close agreement between the two supports the validity of mapping first-principles energies onto the Kanamori crystal-field Hamiltonian, notably at the UHF level of approximation. In the limit of exact exchange the percentage difference between the direct and indirect (mapped) excitation energies is 0.1% and even at the stability limit of the excited states, $F_0 = 0.3$, the difference is only 3%.

IV. CONCLUSIONS

The principal conclusion of this first-principles study of stoichiometric, *nondefective* VO is that the ground electronic state in the rocksalt $(Fm\bar{3}m)$ structure is that of a d^3 high

spin, antiferromagnetic, Mott-Hubbard insulator with an AF_1 spin alignment of the local cation moments. Furthermore, this description remains essentially unchanged for single-particle Hamiltonians ranging from pure UHF, i.e., exact exchange, to exchange-correlation potentials containing down to 10% exact exchange. It is only for the pure DFT potential that the AF_1 phase is predicted to be metallic. Further important conclusions are the following.

(i) For the full range of insulating potentials there is strong spin-lattice interaction with differences in lattice constant of up to 1.6% between AF_1 and FM order.

(ii) The AF_1 lattice constant is predicted to lie in the range (4.35–4.38) Å, with a value of 4.37 Å suggested by direct comparison with a similar range of calculations for the AF_2 alignment of MnO. These values are roughly 7% greater than the reported lattice constants for the stoichiometric, *defective* material.[8,9]

(iii) From a mapping of the total energies of the AF_1, AF_2, and FM alignments onto an Ising spin Hamiltonian containing both direct and superexchange interactions the dominant magnetic interaction is revealed to be the direct coupling of antiferromagnetically aligned nearest-neighbor cation spins, which leads to the stability of the AF_1 phase. While the entire range of insulating potentials favors the AF_1 alignment, there is a fourfold increase in the direct coupling constant from -11.08 to -44.31 meV as the proportion of exact exchange is reduced from the correlated UHF limit down to 10%. This in turn leads to an estimated critical disorder temperature in the range 300–450 K.

(iv) The limitations of such a mapping are exposed by a consideration of the AF_3 structure which fitted coupling constants derived from FM, AF_1, and AF_2 total energies predict to be more stable than AF_1, in contrast to direct total-energy calculations.

(v) From orbital projected densities of states the filled to unfilled gaps are found to depend strongly on the proportion of exact exchange and for the widely examined B3LYP potential are ~ 2.5 eV for the spin-forbidden $xy(\uparrow) \rightarrow xy(\downarrow)$ excitation, ~ 3.0 eV for $xy(\uparrow) \rightarrow z^2(\uparrow)$, and ~ 3.5 eV for V $\rightarrow$O charge transfer. The latter might reasonably be identified with a (strong) absorption edge.

(vi) Variationally stable, highly local crystal-field excited states ranging in energy from ~ 0.6 to ~ 2.7 eV are predicted for exchange-correlation potentials down to 30% exact exchange. All excitations lie below the absorption edge, and from comparisons with the corresponding band excitations, estimates of $\sim 1 - \sim 2$ eV are obtained for the Frenkel localization energy of the crystal-field states.

(vii) A mapping of the excited crystal-field energies onto a Kanamori Hamiltonian leads to values for the (solid-state) Racah B and C parameters, and d-orbital averaged exchange and crystal-field energies. A comparison of fitted and directly calculated energies for the spin-allowed two-electron excitation $xz/yz \rightarrow z^2/x^2-y^2$ confirms the validity of such mapping.

Finally, there is the problematic issue as to whether there is an ''optimum'' or even ''preferred,'' hybridization for VO, as discussed for NiO.[32,43] Clearly the lack of quantitative data for the fully stoichiometric, nondefective material leaves this unresolved at present. However, even for systems such as NiO and MnO, where the data are more plentiful, the values of F_0 that lead to best fit to experiment appear to be both property and system dependent. For NiO, values of F_0 in the region of 0.2–0.4 lead to an energy gap close to the (strong) absorption edge[32,48] and Ising model magnetic coupling constants that are close to the magnon-derived values,[43] although larger values in excess of ~ 0.5 are required for the lattice structure, $d \rightarrow d$ excitation energies and insulating behavior of $Li_xNi_{1-x}O$ $(0 < x \leqslant 0.5)$.[61,75] Furthermore, in the case of MnO, it has recently been shown that a value of F_0 in the region of 0.2–0.3 leads to a direct (magnetic) exchange constant in agreement with that derived from the magnon data, but that a value of F_0 in the region of 0.5–0.6 is required for the superexchange constant.[75] From these and other studies,[75] it is apparent that for the currently reported range of exchange-correlation functionals, hybridization in the midregion, 0.3–0.6, leads to the widest agreement with experiment, so that out final conclusion is that the 'optimum' choice for stoichiometric, nondefective VO is within this region.

ACKNOWLEDGMENT

D.S.M. wishes to thank the EPSRC for financial support, during the tenure of which the work reported here was carried out.

*Author to whom correspondence should be addressed. Email address: wcm@st-and.ac.uk

[1] B. Weckuysen and D. E. Keller, Catal. Today **78**, 25 (2003), and references therein.
[2] K. West, B. Zachauchristiansen, M. J. J. Ostergard, and T. Jacobsen, J. Power Sources **20**, 165 (1987).
[3] J. Verkelis, Z. Bliznikas, K. Breive, V. Dikinis, and R. Saramaitis, Sensors and Actuators A - Physical **68**, 338 (1998).
[4] K. S. Pillai, F. Krumeich, H. J. Muhr, M. Niederberger, and R. Nesper, Solid State Ionics **141**, 185 (2001).
[5] W. Klemm and Z. Grimm, Z. Anorg. Allg. Chem. **250**, 42 (1940).
[6] N. Schönberg, Acta Chem. Scand. (1947–1973) **8**, 221 (1954).
[7] G. Andersson, Acta Chem. Scand. (1947–1973) **8**, 1599 (1954).
[8] R. E. Loehman, C. N. R. Rao, and J. M. Honig, J. Phys. Chem. **73**, 1781 (1969).
[9] M. D. Banus, T. B. Reed, and A. J. Strauss, Phys. Rev. B **5**, 2775 (1972).
[10] F. J. Morin, Phys. Rev. Lett. **3**, 34 (1959).
[11] I. G. Austin, Philos. Mag. **7**, 961 (1962).
[12] S. Kawano, K. Kosuge, and S. Kachi, J. Phys. Soc. Jpn. **21**, 2744 (1966).
[13] M. D. Banus and T. B. Reed, in *The Chemistry of Extended Defects in Non-Metallic Solids*, edited by L. Eyring and M. O'Keeffe (North-Holland, Amsterdam, 1970), p. 488.
[14] P. V. Gel'd, S. I. Alyamovskii, and I. I. Matveenko, Zh. Strukt. Khim. **2**, 301 (1961).

[15] C. M. Ariya, B. Y. Brach, and V. A. Vladimirova, Vestn. Leningr. Univ., Fiz., Khim. **22**, 157 (1967).
[16] H. Takei and S. Koide, J. Phys. Soc. Jpn. **24**, 1394 (1968).
[17] S. Kawano, K. Kosuge, and S. Kachi, J. Phys. Soc. Jpn. **27**, 1076 (1969).
[18] J. M. Honig, W. E. Wahnsiedler, M. D. Banus, and T. B. Reed, J. Solid State Chem. **2**, 74 (1970).
[19] K. Suzuki and S. Takeuchi, in *Ferrites '70*, Proceedings of the International Conference, edited by Y. Hoshino (University Park Press, Baltimore, MD, 1971), p. 568.
[20] M. I. Aivazov, J. A. Domashnev, A. G. Sarkisyan, and S. V. Gurov, Izv. Akad. Nauk SSSR, Neorg. Mater. **8**, 1069 (1972).
[21] W. E. Wahnsiedler and J. M. Honig, J. Phys. Chem. Solids **33**, 1836 (1972).
[22] A. H. Wilson, *The Theory of Metals* (Cambridge University Press, Cambridge, 1954).
[23] J. C. Slater, Phys. Rev. **81**, 385 (1951).
[24] T. E. Norwood and J. L. Fry, Phys. Rev. B **2**, 472 (1970).
[25] L. F. Mattheiss, Phys. Rev. B **5**, 290 (1972); **5**, 290 (1972).
[26] A. Neckel, P. Rastl, R. Eibler, P. Weinberger, and K. Schwarz, J. Phys. C **9**, 579 (1976).
[27] U. von Barth and L. Hedin, J. Phys. C **5**, 1629 (1972).
[28] O. K. Andersen, H. L. Skriver, H. Nohl, and B. Johansson, Pure Appl. Chem. **52**, 93 (1979).
[29] W. C. Mackrodt, N. M. Harrison, V. R. Saunders, N. L. Allan, M. D. Towler, E. Apra, and R. Dovesi, Philos. Mag. A **68**, 653 (1993).
[30] J. Zaanen, G. A. Sawatzky, and J. W. Allen, Phys. Rev. Lett. **55**, 418 (1985).
[31] K. Terakura, T. Oguchi, A. R. Williams, and J. Kübler, Phys. Rev. B **30**, 4734 (1984).
[32] T. Bredow and A. R. Gerson, Phys. Rev. B **61**, 5194 (2000).
[33] Ph. Dufek, P. Blaha, V. Sliwko, and K. Schwarz, Phys. Rev. B **49**, 10 170 (1994).
[34] Z.-X. Shen, R. S. List, D. S. Dessau, B. O. Wells, O. Jepsen, A. J. Arko, R. Barttlet, C. K. Shih, F. Parmigiani, J. C. Huang, and P. A. P. Lindberg, Phys. Rev. B **44**, 3604 (1991).
[35] T. C. Leung, C. T. Chan, and B. N. Harmon, Phys. Rev. B **44**, 2923 (1991).
[36] W. E. Pickett, Rev. Mod. Phys. **61**, 433 (1989).
[37] A. Svane and O. Gunnarsson, Phys. Rev. Lett. **65**, 1148 (1990).
[38] Z. Szotek, W. M. Temmerman, and H. Winter, Phys. Rev. B **47**, 4029 (1993).
[39] V. I. Anisimov, J. Zaanen, and O. K. Andersen, Phys. Rev. B **44**, 943 (1991).
[40] V. I. Anisimov, I. V. Solovyev, M. A. Korotin, M. T. Czyzyk, and G. A. Sawatzky, Phys. Rev. B **48**, 16 929 (1993).
[41] V. I. Anisimov, F. Aryasetiawan, and A. I. Liechtenstein, J. Phys.: Condens. Matter **9**, 767 (1997).
[42] C. Leung, M. Weinert, P. B. Allen, and R. M. Wentzcovitch, Phys. Rev. B **54**, 7857 (1996).
[43] I. P. R. Moreira, F. Illas, and R. L. Martin, Phys. Rev. B **65**, 155102 (2002).
[44] A. D. Becke, J. Chem. Phys. **98**, 5648 (1993).
[45] C. Adamo, M. Ernzerhof, and G. E. Scuseria, J. Chem. Phys. **112**, 2643 (2000).
[46] C. Lee, W. Yang, and R. G. Parr, Phys. Rev. B **37**, 785 (1988).
[47] S. H. Vosko, L. Wilk, and M. Nusair, Can. J. Phys. **58**, 1200 (1980).
[48] J. Muscat, A. Wander, and N. M. Harrison, Chem. Phys. Lett. **342**, 397 (2001).
[49] J. Kanamori, J. Phys. Chem. Solids **10**, 87 (1959).
[50] J. S. Griffith, *The Theory of Transition Metal Ions* (Cambridge University Press, Cambridge, 1964).
[51] V. R. Saunders, R. Dovesi, C. Roetti, M. Causà, N. M. Harrison, R. Orlando, and C. M. Zicovich-Wilson, CRYSTAL98 User's Manual (University of Torino, Torino, 1998).
[52] F. D. Murnaghan, Proc. Natl. Acad. Sci. U.S.A. **30**, 244 (1944).
[53] P. R. Son and R. A. Bartels, J. Phys. Chem. Solids **33**, 819 (1972).
[54] M. R. Notis, R. M. Spriggs, and W. C. Hahn, J. Appl. Phys. **44**, 4165 (1973).
[55] T. Kondo, T. Yagi, Y. Syono, Y. Noguchi, T. Atou, T. Kikegawa, and O. Shimomura, J. Appl. Phys. **87**, 4153 (2000).
[56] R. L. Clendenen and H. G. Drickamer, J. Chem. Phys. **44**, 4223 (1966).
[57] R. Jeanloz and A. Rudy, J. Geophys. Res. **92**, 11 433 (1987).
[58] S. L. Webb, I. Jackson, and J. D. FitzGerald, Phys. Earth Planet. Inter. **52**, 117 (1988).
[59] Y. Noguchi, K. Kusaba, K. Fukuokaand, and Y. Syono, Geophys. Res. Lett. **23**, 1469 (1996).
[60] M. D. Towler, N. L. Allan, N. M. Harrison, V. R. Saunders, W. C. Mackrodt, and E. Aprà, Phys. Rev. B **50**, 5041 (1994).
[61] F. Corà, M. Alfredsson, G. Mallia, D. S. Middlemiss, W. C. Mackrodt, R. Dovesi, and R. Orlando, *Structure and Bonding* (Springer-Verlag, Berlin, 2004).
[62] A. Freitag, V. Staemmler, D. Cappus, C. A. Ventrice, K. Al Shamery, H. Kuhlenbeck, and H.-J. Freund, Chem. Phys. Lett. **210**, 10 (1993).
[63] C. de Graaf, H. Broer, and W. C. Nieuwpoort, Chem. Phys. **208**, 35 (1996).
[64] M. Geleijins, C. de Graaf, H. Broer, and W. C. Nieuwpoort, Surf. Sci. **421**, 106 (1999).
[65] C. Kittel, *Introduction to Solid State Physics*, 6th ed. (Wiley, New York, 1986).
[66] W. C. Mackrodt and C. Noguera, Surf. Sci. **457**, L386 (2000).
[67] B. Fromme, M. Schmitt, E. Kisker, A. Gorschlüter, and H. Merz, Phys. Rev. B **50**, 1874 (1994).
[68] B. Fromme, M. Möller, Th. Anschütz, C. Bethke, and E. Kisker, Phys. Rev. Lett. **77**, 1548 (1996).
[69] R. Liu, D. Salamon, M. V. Klein, S. L. Cooper, W. C. Lee, S. W. Cheong, and D. M. Ginsberg, Phys. Rev. Lett. **71**, 3709 (1993).
[70] J. P. Falck, J. D. Perkins, A. Levy, M. A. Kastner, J. M. Graybeal, and R. J. Birgeneau, Phys. Rev. B **49**, 6246 (1994).
[71] P. Kuiper, J. H. Guo, C. Såthe, L.-C. Duda, J. Nordgren, J. J. M. Pothuizen, F. M. F. de Groot, and G. A. Sawatzky, Phys. Rev. Lett. **80**, 5204 (1998).
[72] S. Sugano, Y. Tanabe, and H. Kamimura, *Multiplets of Transition-Metal Ions in Crystals* (Academic Press, New York, 1970).
[73] R. E. Cohen, I. I. Mazin, and D. G. Isaak, Science **275**, 654 (1997).
[74] J. Badro, V. V. Struzhkin, J. Shu, R. J. Hemley, H. K. Mao, C. C. Kao, J.-P. Rueff, and G. Shen, Phys. Rev. Lett. **83**, 4101 (1999).
[75] W. C. Mackrodt and D. S. Middlemiss (unpublished).